This is a repository copy of *Conceptual design of the early implementation of the NEutron Detector Array (NEDA) with AGATA*.

White Rose Research Online URL for this paper:
https://eprints.whiterose.ac.uk/101631/

Version: Accepted Version

Article:

Conceptual design of the early implementation of the NEutron Detector Array (NEDA) with AGATA

Tayfun Hüyük

Instituto de Física Corpuscular, CSIC - Universidad de Valencia,
E-46980 Paterna (Valencia), Spain

Antonio Di Nitto

Istituto Nazionale di Fisica Nucleare, Sezione di Napoli, I-80126 Napoli, Italy
Johannes Gutenberg-Universität Mainz, D-55099 Mainz, Germany

Grzegorz Jaworski

Istituto Nazionale di Fisica Nucleare, Laboratori Nazionali di Legnaro,
I-35020 Legnaro (PD), Italy

Andrés Gadea

Instituto de Física Corpuscular, CSIC - Universidad de Valencia,
E-46980 Paterna (Valencia), Spain

José Javier Valiente-Dobón

Istituto Nazionale di Fisica Nucleare, Laboratori Nazionali di Legnaro,
I-35020 Legnaro (PD), Italy

Johan Nyberg

Department of Physics and Astronomy, Uppsala University, SE-75120 Uppsala, Sweden

Marcin Palacz

Heavy Ion Laboratory, University of Warsaw, 02-093 Warsaw, Poland

Pär-Anders Söderström

RIKEN Nishina Center, 351-0198 Saitama, Japan

Ramon Jose Aliaga-Varea

Instituto de Física Corpuscular, CSIC - Universidad de Valencia,
E-46980 Paterna (Valencia), Spain
I3M, Universidad Politécnica de Valencia, E-46022 Valencia, Spain

Giacomo de Angelis

Istituto Nazionale di Fisica Nucleare, Laboratori Nazionali di Legnaro,
I-35020 Legnaro (PD), Italy

1

Ayşe Ataç
Department of Physics, Faculty of Sciences, Ankara University, 06100 Ankara, Turkey
The Royal Institute of Technology, SE-10691 Stockholm, Sweden

Javier Collado
Department of Electronic Engineering, University of Valencia,
E-46100 Burjassot (Valencia), Spain

Cesar Domingo-Pardo
Instituto de Física Corpuscular, CSIC - Universidad de Valencia,
E-46980 Paterna (Valencia), Spain

Francisco Javier Egea
Department of Electronic Engineering, University of Valencia,
E-46100 Burjassot (Valencia), Spain

Nizamettin Erduran
Faculty of Engineering and Natural Sciences, Istanbul Sabahattin
Zaim University, 34303 Istanbul, Turkey

Sefa Ertürk
Department of Physics, Faculty of Science and Arts,
University of Nigde, 51240 Niğde, Turkey

Gilles de France
GANIL, CEA/DSAM and CNRS/IN2P3, F-14076 Caen, France

Rafael Gadea
I3M, Universidad Politécnica de Valencia, E-46022 Valencia, Spain

Vicente González
Department of Electronic Engineering, University of Valencia,
E-46100 Burjassot (Valencia), Spain

Vicente Herrero-Bosch
I3M, Universidad Politécnica de Valencia, E-46022 Valencia, Spain

Ayşe Kaşkaş
Department of Physics, Faculty of Sciences, Ankara University,
06100 Ankara, Turkey

Victor Modamio
Istituto Nazionale di Fisica Nucleare, Laboratori Nazionali di Legnaro,
I-35020 Legnaro (PD), Italy

Marek Moszynski
National Centre for Nuclear Research, 05-400 Otwock-Swierk, Poland

Enrique Sanchis
Department of Electronic Engineering, University of Valencia,
E-46100 Burjassot (Valencia), Spain

Andrea Triossi
Istituto Nazionale di Fisica Nucleare, Laboratori Nazionali di Legnaro,
I-35020 Legnaro (PD), Italy

Robert Wadsworth
Department of Physics, University of York,
Heslington, YO10 5DD York, United Kingdom

June 20, 2016

Abstract

The NEutron Detector Array (NEDA) project aims at the construction of a new high-efficiency compact neutron detector array to be coupled with large γ-ray arrays such as AGATA. The application of NEDA ranges from its use as selective neutron multiplicity filter for fusion-evaporation reaction to a large solid angle neutron tagging device. In the present work, possible configurations for the NEDA coupled with the Neutron Wall for the early implementation with AGATA has been simulated, using Monte Carlo techniques, in order to evaluate their performance figures. The goal of this early NEDA implementation is to improve, with respect to previous instruments, efficiency and capability to select multiplicity for fusion-evaporation reaction channels in which 1, 2 or 3 neutrons are emitted. Each NEDA detector unit has the shape of a regular hexagonal prism with a volume of about 3.23 litres and it is filled with the EJ301 liquid scintillator, that presents good neutron-γ discrimination properties. The simulations have been performed using a fusion-evaporation event generator that has been validated with a set of experimental data obtained in the ^{58}Ni + ^{56}Fe reaction measured with the Neutron Wall detector array.

1 Introduction

Contemporary nuclear physics experiments aim to investigate the structure of exotic nuclei lying far from the valley of β stability. One of the most successful methods for producing such exotic nuclei is to use fusion-evaporation reactions with stable or radioactive beams and stable targets. The most exotic neutron-deficient nuclei are produced in extremely weak reaction channels after the emission of two or more neutrons from the compound nuclei. In order to perform high resolution γ-ray spectroscopy of such exotic systems, as for instance in the case of ^{92}Pd [1], the identification of the reaction channel requires, in addition to the high efficiency and selectivity, the determination of the neutron multiplicity. In neutron detectors like NEutron Detector Array (NEDA), one of the major critical issues in the determination of the neutron multiplicity is the scattering of neutrons between the different detectors of the array. The neutron scattering gives rise to signals in more than one detector, creating an ambiguity in the actual number of neutrons detected (neutron cross-talk). One important goal in the design of new neutron detection filters, such as NEDA, is to minimise the neutron cross-talk and to increase the efficiency for detecting 2 or 3 neutrons compared to existing arrays, e.g. the Neutron Wall [2, 3] and the Neutron Shell [4].

Moreover, NEDA will make use of digital electronics and state-of-the-art digital signal processing based on NUMEXO2 cards [5, 6]. With this in mind, considerable effort has been ex-

pended recently in studying digital timing [7], fast digital data acquisition cards [8] and digital pulse shape discrimination [9, 10].

The size of the single detector unit and the scintillation material used for the neutron detection are important factors in order to optimise the performance of the full array. A detailed study, using Monte Carlo simulations of a detector unit filled with liquid scintillator, reported the optimum size that is sufficient for the detection of neutrons typically emitted in fusion-evaporation reactions [11]. The outcome of that work was used to decide the dimensions of a single NEDA detector.

This paper is organised as follows: In Sec. 2 the description of the NEDA detectors will be presented in more detail. In Sec. 3, the simulations to evaluate the performance of the first implementation of NEDA together with the Neutron Wall will be discussed. The geometry will be defined in Sec. 4. The simulations performed to determine the neutron efficiency for the cases of isotropic emission from the ^{252}Cf source and for a fusion-evaporation reaction, are presented and discussed in the same section.

2   Design of the NEDA detectors

NEDA is conceptually designed as a flexible array with identical detector units able to adapt to different experimental setups. It is expected to be coupled with complementary Ge detector instrumentation like AGATA [12], EXOGAM2 [13] or GALILEO [14]. A regular hexagon was chosen as the starting point for the design of the NEDA geometry since it is the most suitable polygon for both clustering detectors and coupling to a circularly shaped photomultiplier tube (PMT), minimising the uncovered area by the PMT. NEDA detectors will have the shape of a uniform hexagonal prism, see Fig. 1. The optimum depth of the detector units, evaluated using GEANT4 simulations, is 20 cm as discussed in Ref. [11]. The side length of the hexagon is 84 mm, suitable for the largest commonly available photomultiplier tubes with 5 inch diameter. The volume of each detector is 3.23 litres to be filled with EJ301 liquid scintillator. An aluminium canning with a thickness of 3 mm is used in order to provide sufficient mechanical stability of the detector.

The broad experimental conditions expected for NEDA, using both stable and radioactive high intensity beams, require a modular concept of the overall design. In addition to modularity, three basic conditions are to be considered for the design of the array, that have implications in the design of the detectors:

1. Efficiency: to be maximised within the geometrical coverage.

2. Target-to-detector distance: large enough for neutron-γ discrimination by Time-Of-Flight (TOF)

3. Granularity: to maximize the efficiency for the reaction channels with neutron multiplicity is at least 1.

The possibility to have a flexible array that can change the distance between the target and the detectors, make this array more adaptable to the needs of the different physics cases. It allows to improve the neutron-γ discrimination based on TOF measurements, but also to increase the neutron energy resolution. Clearly, increasing the distance to the target would require a sizeable number of additional detectors for the same angular coverage.

3   Monte Carlo simulations and analysis procedure

The main goal of this paper is to report on the performance figures of an early implementation of NEDA combined with the Neutron Wall and AGATA. The evaluation of such figures requires the use of Monte Carlo techniques. The Monte Carlo simulations presented in this manuscript were carried out using GEANT4 [15] and the AGATA Simulation Package (ASP) [12, 16]. The
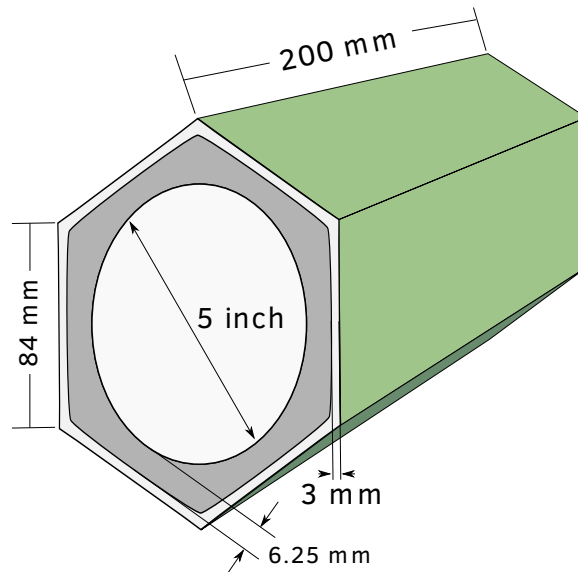
4

Figure 1: Schematic picture of the NEDA detector unit (color online).

ASP was chosen since it is compatible with the existing simulations of AGATA and other γ-ray detector arrays. With the ASP, it is possible to implement different geometrical configurations into the simulations and to select a number of essential parameters, e.g. detector material, source position, angular distribution of emitted particles, etc. The performance of the proposed array has been simulated for a ^{252}Cf source that emits neutrons isotropically and for the fusion-evaporation reaction ^{58}Ni + ^{56}Fe in which the neutrons are distributed according to the reaction kinematics. In GEANT4 the physical conditions of the simulations are mimicked by the so called "event generator", which will be introduced in the next subsection.

3.1 Event generators

As mentioned before, two different event generators have been used, one corresponding to a ^{252}Cf source emitting neutrons isotropically and the other to a realistic fusion-evaporation reaction. The neutron energy distribution of a ^{252}Cf source was produced by the built-in event generator of GEANT4 an by using the expression (see Eq. 1) deduced in Ref. [17] with T = 1.42 MeV and E given in MeV.

$$N(E) = E^{1/2} e^{-E/T}. \tag{1}$$

Regarding the realistic fusion-evaporation reaction events, the Monte Carlo Hauser-Feshbach code LILITA_N97 [18] has been used to calculate the physical parameters of the neutron emission on event-by-event basis. The code includes several options for transmission coefficients, yrast line, level density and nuclear deformations, some of which are described and discussed in Ref. [19, 20]. In LILITA_N97, the de-excitation of the compound nucleus is modelled through a multistep emission of light particles (neutrons, protons and α-particles) adopting the Hauser-Feshbach formulation of the statistical model in conjunction with the Monte Carlo method. The program produces energy spectra and angular distributions in the laboratory frame for light particles and evaporation residues. Furthermore, for this work, a new prescription for the transmission coefficients based on the Optical Model (OM) was implemented in the code. The global parametrisation of Koning and Delaroche was adopted for neutrons and protons [21]. Due to the inclusion of the N-Z dependence, the OM parameters are well suited for calculations

involving nuclei far from stability. The validation of this second event generator will be discussed in terms of neutron efficiency and angular distribution in the following subsection.

3.2 Verification of the fusion-evaporation reaction event generator

The modeling of a fusion-evaporation reaction is complex and depends on several parameters that are not always known. In order to validate our simulations, the event generator has been verified by comparing a Neutron Wall measurement with a simulation of the same setup. A representation of the GEANT4 model of the Neutron Wall system is shown in Fig. 2. In order to get a realistic comparison between the real data and the simulations, most of the materials between the target and the Neutron Wall were included, namely two concentric beam pipes of stainless steel with a thickness of 2 mm and a length of 250 mm together with a standard CF100 vacuum flange which were used as a beam dump in the experiment (see inset in Fig. 2). The energy loss inside the target was also taken into account. A data set measured with the Neutron Wall in which a ^{58}Ni beam at 220 MeV impinging on a ^{56}Fe target with a thickness of 10 mg cm^{-2}, was used for comparison. The choice of this reaction was motivated by the existence of a data set used earlier for the characterisation of the Neutron Wall detector array [3]. Moreover, the characteristics of this reaction are quite similar to those that we intend to use in future experiments with NEDA.

In the experiment, the Neutron Wall was coupled to the EUROBALL γ-ray spectrometer [22]. The trigger condition required at least two Compton-suppressed γ-rays in the HPGe detectors and there was no trigger condition on the Neutron Wall. The experimental energy threshold of the neutron detectors were determined using the calibration runs performed with a ^{207}Bi γ-ray source collected just before the experiment. The thresholds were determined for each Neutron Wall detector. The average value of the thresholds of the 43 operational detectors was determined to be 150 keVee. In order to validate the event generator we will make a comparison of the experimental TOF distributions measured in the aforementioned experiment for the various polar angles of the Neutron Wall with the GEANT4 simulations.

Figure 3 shows the measured and simulated TOF spectra for the six different θ angles of the Neutron Wall, see Table 1. The experimental data were collected using a common stop for the neutron detectors, therefore the time axis runs from right to left. The center of the γ-ray time distribution has been taken as time reference (t = 0 ns in the spectra). The rescaling between experimental and simulated data was performed using the ratio between the total number of neutrons in the experimental and simulated TOF spectra.

Table 1: Grouping of the Neutron Wall detectors according to their polar angle θ.

Group	n. Detectors	n. Working Detectors	θ (deg.)
0	5	4	57.21
1	20	17	47.20
2	5	3	34.87
3	5	5	30.30
4	10	10	18.54
5	5	4	6.90

The simulated spectra are obtained: *i*) using the measured experimental thresholds and *ii*) taking into account the seven detectors that were inoperative during the experiment. However, the presence of the inoperative detectors were taken into account to simulate the real setup, since they influence, in particular, the events including scattering. In order to reproduce this particular set of experimental data, several values of the level density parameter a in the range
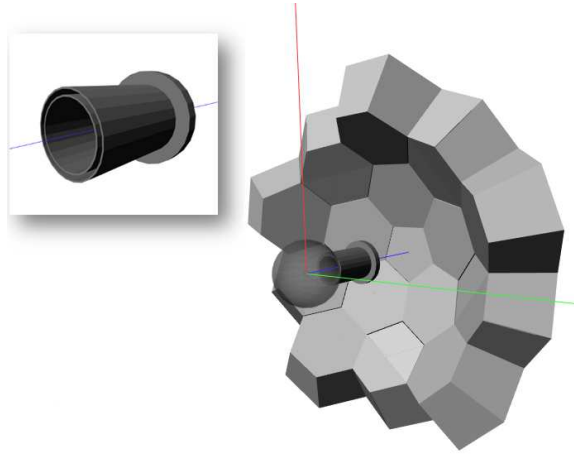
Figure 2: View of the Neutron Wall (light grey) with the beam pipe and beam dump after the target (dark grey) as modelled by GEANT4. The inset in the upper left corner shows in some detail the materials used in the beam pipe and beam dump. The target is positioned in the center of the spherical reaction chamber.

from $A/12$ to $A/6$ were considered in the `LILITA_N97` code. The best agreement was obtained with $a = A/8$. Prescriptions with a dependency of the parameter a and of the symmetry energy on the neutron-proton mass asymmetry were not considered, because their effects are negligible on the inclusive neutron energy spectra and angular distributions. Nevertheless, these dependencies may be important for the determination of the neutron energy spectra for very exotic nuclei and the cross sections of the evaporation residues are predicted to be more affected [23]. However, these are beyond the scope of this publication and will be studied in a future work.

Large discrepancies between experimental and simulated data with plain results of `LILITA_N97` are shown in Fig. 3. The discrepancy is especially large for the detectors at forward angles ($\theta < 20°$). The reason for this is the simulated neutrons (grey spectra) have lower mean energies than the experimental ones (black spectra) as can be seen in Fig. 3 where the maximum of the experimental distribution is shifted to lower TOF values. Furthermore, the ratio between detected -simulated and experimental- number of neutrons is rather different at the smaller and larger polar angles. The ring at $6.9°$ shows the largest disagreement. In order to improve the agreement of the simulated and experimental data, the center-of-mass energy of the evaporated light particles had to be increased by 800 keV in `LILITA_N97`. This energy was subtracted from the excitation energy of the nucleus after each neutron emission, in order to keep the correct competition between different decay channels. The physical reason behind the disagreement, concerning the energy of the evaporated neutron, between the measurement and the statistical model is not fully understood. The statistical model parameter a, the transmission coefficients and the yrast lines cannot produce such a large effect on the energy of the emitted neutrons. One possibility could be a different distribution of the decay channels between experiment and simulations, but this could not be verified using the present data set, due to low statistics. This remains an open question, that goes beyond the goal of the present work and is planned to be investigated in future experiments. In Fig. 3, the simulated TOF distributions are shown also after applying the 800 keV correction discussed above (red spectra). The standard deviation of the γ TOF distribution in the experimental data was found to be $\sigma=2.21$ ns, thus the Gaussian smearing function has been applied to the simulated data. As seen in the figure, the agreement

is quite good and therefore we conclude that the event generator can be used to determine the performance figures of NEDA for the fusion-evaporation reaction.

Figure 4 shows the experimental and simulated neutron differential detection efficiency as a function of the polar angle θ for the Neutron Wall. This relative neutron detection efficiency was calculated according the expression:

$$\varepsilon_{\mathrm{rel},\theta} = \varepsilon_{1\mathrm{n}} \frac{N_\theta}{N_{\mathrm{NW}}} \frac{1}{\Omega_\theta}, \tag{2}$$

where $\varepsilon_{1\mathrm{n}}$ is the efficiency to detect at least one-neutron, N_{NW} the number of detected neutrons in the whole array, N_θ the number of detected neutrons in the ring at angle θ and Ω_θ the solid angle covered by the detectors at that angle. The solid angle correction in Eq. 2 is necessary since the detector volume at every polar angle varies, and this effect needs to be excluded for a clearer comparison.

In the case of fusion-evaporation reactions, one would expect a monotonic decrease of the neutron efficiency as a function of the θ angle due to the neutron angular distribution in the laboratory reference system. However, as a result of the neutron scattering with the material of the beam dump shown in Fig. 2, there is a clear reduction of the relative efficiency at the forward angles both experimentally and in the simulations. The simulated and experimental curves show the same behaviour as a function of θ. The experimental data points are, however, lower than the simulated ones by a constant factor for the whole angular range. The origin of this mismatch might be due to several factors, e.g. from different events close in time (pile-up) depending on the structure of the beam pulses as well as from the same event in case of multiple hits of γ-rays in high multiplicity cascades, causing sum up of the signals, which makes neutrons undistinguishable from γ-rays.

In order to obtain an acceptable level of agreement between simulations and experiment, a correction factor with a value of 0.772(1) has been introduced. This factor was calculated using the experimental neutron detection efficiency of the full Neutron Wall, reported to be 26(6) % in Ref. [3], and the simulated neutron efficiency, which was 33.7(1) % according to the present work. Figure 4 shows a perfect overlap for the whole angular range when the correction factor is used.

3.3 Handling of the scattered events

As mentioned before, in a neutron detector array with a compact geometry, such as NEDA, the probability of neutron cross-talk between detectors is rather large. In the Neutron Wall detector system the simulated neutron cross-talk is estimated to be 12% in fair agreement with the previous estimates [2, 3]. This leads to an ambiguity regarding the real number of neutrons interacting in the array. In order to decrease this ambiguity and to optimise the two- and three-neutron efficiency, a method based on the correlation between the detector centroids (Δr) and the TOF (Δt) difference of two fired detectors in the array is commonly used [3, 24]. Each pair of coincident neutron signals is evaluated to determine whether they are produced by two different neutrons or by the scattering of a single one (See Fig. 5). If the difference Δt is large enough to cover the distance Δr, assuming a realistic range for the neutron energy, the two signals are assigned to the neutron cross-talk category, i.e. a single neutron was detected. Otherwise, they are assigned to the real two neutron events. This procedure can be extended to all possible combinations of two pairs of detectors fired in each event.

Figure 6 shows the distribution of Δr versus Δt for simulated single neutron events emitted in a fusion-evaporation reaction. By definition, all these data points are associated to neutron cross-talk events and the observed distribution in Δt is due to the differences in the neutron velocities, and the velocities are independent from the geometry of the detector system. Events in which two real neutrons are detected should give counts inside the gate. The edge of the gate represents the largest neutron velocity for which a crosstalk event is defined and therefore
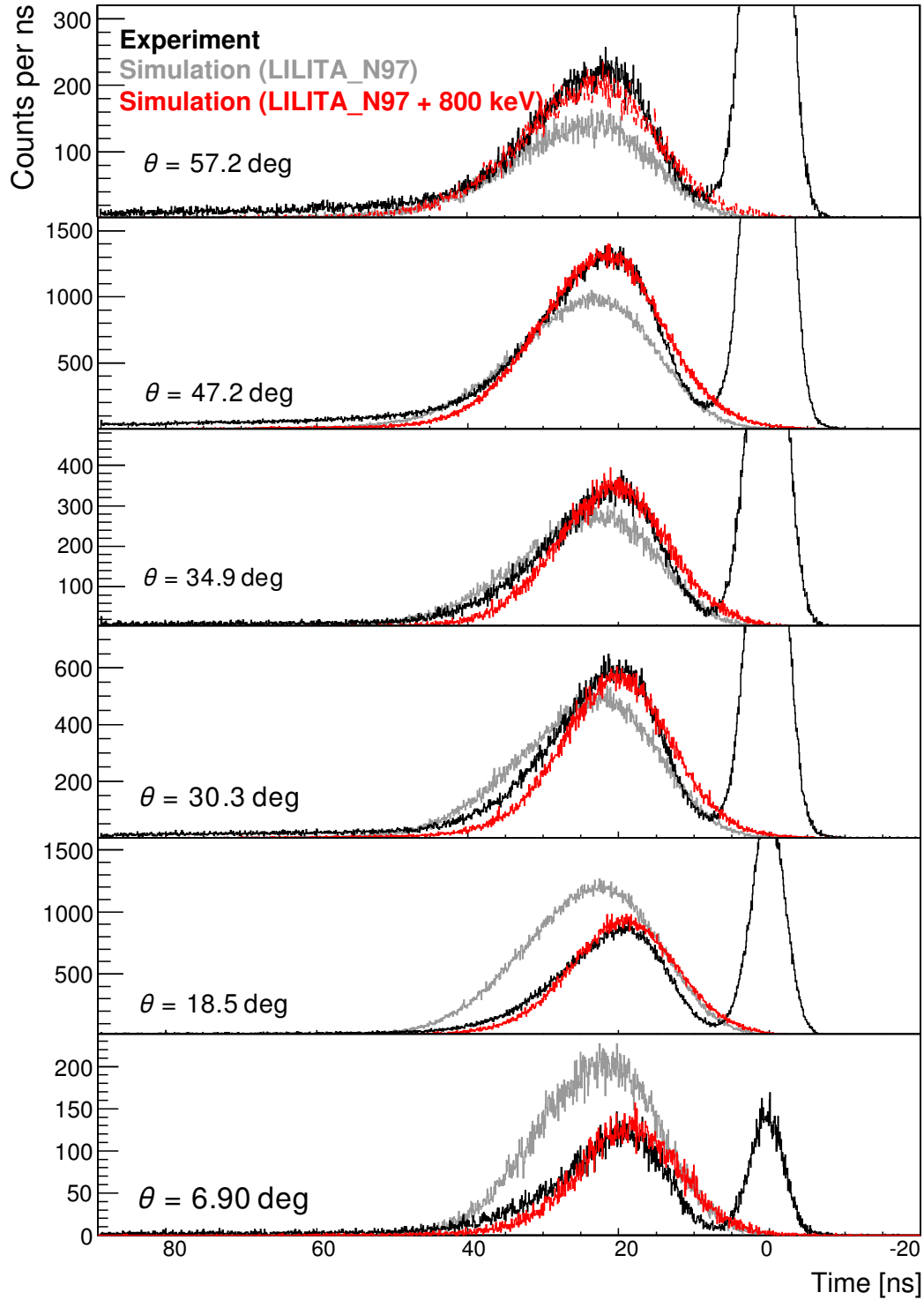
Figure 3: Simulated and experimental TOF spectra for the six different θ angles of the Neutron Wall. TOF increases from right to left. Gamma rays were not included in the simulations. The large Gaussian-shaped peak in the experimental spectra, centered at time 0 ns and with a width of $\sigma = 2.21$ ns, is due to γ rays. For the comparison of the simulated and experimental data, the former were smeared with a Gaussian distribution with the same width as the γ-ray peak. The initial simulated TOF spectra are shown in grey colour. The simulated TOF spectra after the center-of-mass energy of the evaporated neutrons was increased by 800 keV are shown in red colour. The experimental data are shown in black colour (color online).
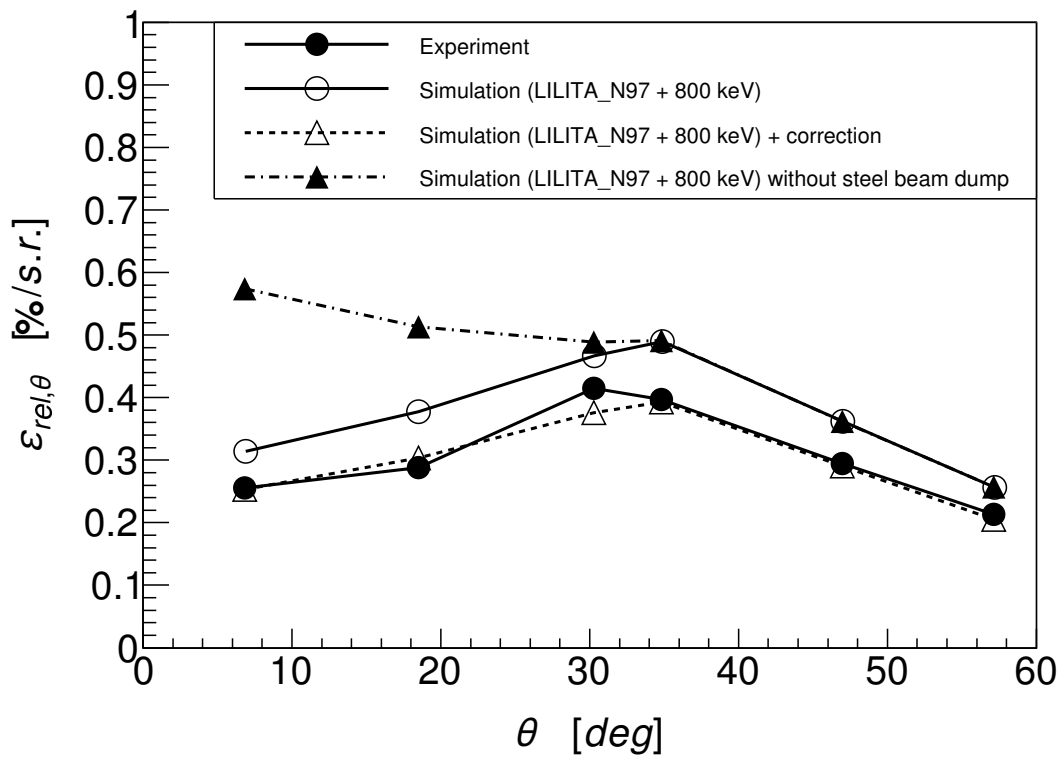
Figure 4: Experimental and simulated neutron detection efficiency per solid angle as a function of the polar angle θ of the Neutron Wall. The efficiency at the forward angles decreases due to the stainless steel beam dump shown in Fig. 2.
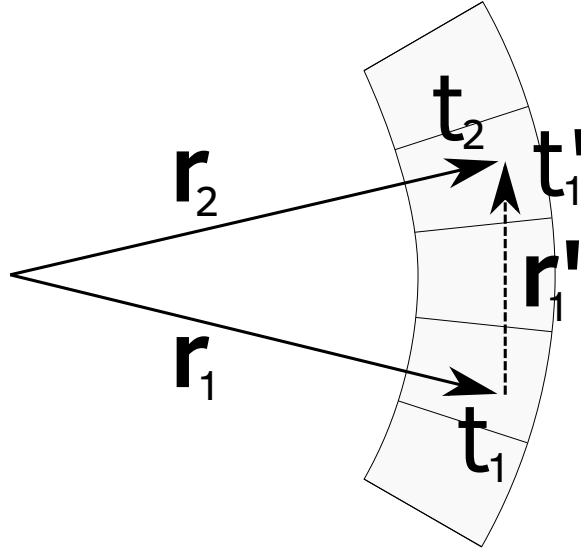
Figure 5: Schematic view of the Neutron Wall, showing two real neutron events with an associated time t_1 and t_2 and a scattered event t'_1. The difference $t_1 - t_2$ is smaller than a scatter event $t_1 - t'_1$, in average, for the vast majority of events.

for a given neutron energy spectrum the form of the gate is independent of the geometry. It can be seen that the gate is not symmetric around the $\Delta t = 0$. This is because detectors are sorted with a criterion that the interaction which left more energy in the detector should be the one that occurs first. Thus the positive Δt values are more frequent than the negative ones. A few events can be observed inside the gate. These events are due to neutrons with a very large energy. They correspond to events with velocities larger than the one defined by the gate, therefore they cannot be discriminated from the real events. This leakage, which is almost negligible, is only about $0.05\,\%$.

4   Early implementation of NEDA to be coupled with AGATA: Design and results of the simulations

An early implementation of NEDA, together with the Neutron Wall, is proposed to be coupled to AGATA at GANIL. The use of the Neutron Wall detectors in combination with NEDA detectors has been considered in order to maximise the number of detectors and therefore the efficiency of the setup. The coupling of both arrays will provide the best achievable performance compared to the case of the Neutron Wall standalone. Two configurations have been proposed that are shown in Fig. 7. The reason to consider these two configurations are related to the geometry of the Neutron Wall detectors - these are more compact in the configuration shown in Fig. 7-a and in a "ring" at ninety degrees in the configuration shown in Fig. 7-b. The basic properties of both configurations, together with those of the Neutron Wall alone are listed in Table 2.

In the setup shown in Fig. 7-a, the Neutron Wall is translated 180 mm away from its nominal position in the downstream beam direction, i.e. the front faces of the pentagonal detectors are at 690 mm from the target position. The 50 NEDA detector units are placed at 510 mm, 17 are at $60.5°$, 16 are at $74°$, and 17 are at $87.5°$ with respect to the beam direction, in order to cover a larger solid angle in the forward direction. On the other hand, in the setup shown in

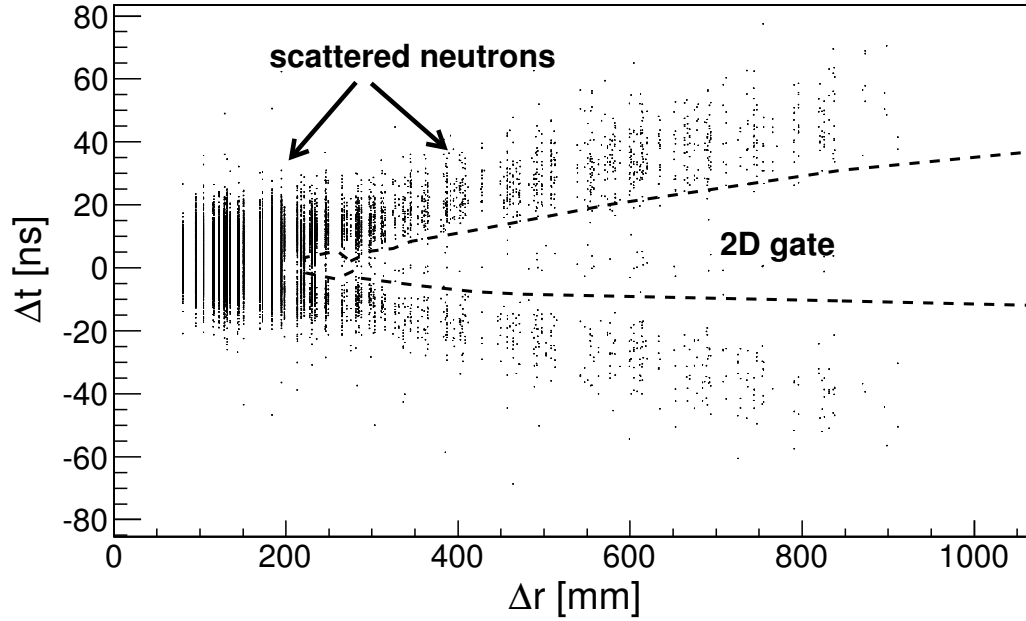Figure 6: Δr-Δt plot for simulated one neutron events from the fusion-evaporation reaction, described in the text. The two dimensional gate shown with a dashed line corresponds to the position where the real detection of two- and three-neutron events would be located.

Table 2: Summary of the basic properties of the Neutron Wall and the NW + NEDA.

Geometry		Granularity	Solid angle [sr]	Volume/unit [litres]	Total volume [litres]	Radial distance to target [m]
Neutron Wall (NW)		50	$\approx 1.00\pi$	(*)	149.5	0.51
NW + NEDA	NEDA	50	$\approx 1.63\pi$	3.23	311.0	0.51
	NW	50		(*)		0.69
NW-ring + NEDA	NEDA	51	$\approx 1.60\pi$	3.23	308.7	(**)
	NW-ring	45		3.20		0.51

(*) Volume of each segment of the Neutron Wall detectors is 1.1 l for the segments of the pentagonal detector and 3.2 l for the segments of the hexagonal detectors.
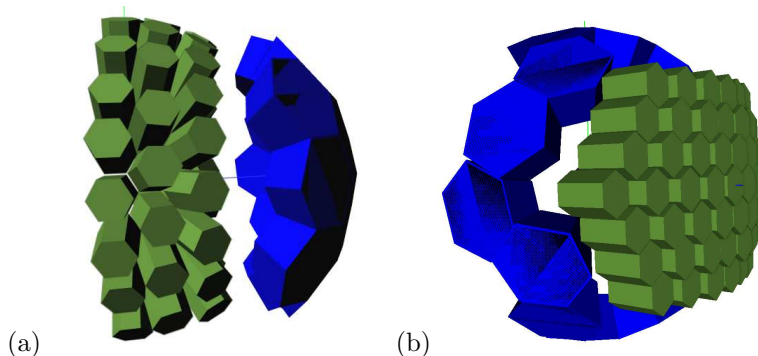(**) The distance between the central detector of the NEDA array and the target position is 0.57 m.

Figure 7: The proposed geometries of the NEDA array - left-hand-side in (a), right-hand-side in (b) - coupled to the Neutron Wall - right-hand-side in (a), left-hand-side in (b) - for the AGATA campaign at GANIL (color online). See text for details.

Fig. 7-b, the hexagonal units of the Neutron Wall are placed at θ angles between $60°$ and $90°$. The target-to-detector distance of the Neutron Wall is kept at its original position, i.e. 510 mm. The 51 NEDA unitary cells are placed at between $\theta = 0°$ and $\theta = 60°$, covering a solid angle of about $\approx 0.7\pi$ sr in the forward position. The central detector unit of NEDA is placed at 570 mm from the target position.

Tables 3 and 4 show the simulated one-, two- and three-neutron efficiencies for neutrons emitted from a ^{252}Cf source and from the fusion-evaporation reaction ^{58}Ni + ^{56}Fe, respectively. The efficiencies are calculated according to the following expression:

$$\varepsilon_{mn} = \frac{N_{\geq m}}{N_{emitted}}, \tag{3}$$

where $N_{\geq m}$ is the number of events that includes neutrons identified with multiplicity at least m. This specific definition of efficiency assumes that multiplicities bigger than the number of neutrons emitted m is only due to scattered neutrons which is preferred in the experiments aiming nuclei far from stability in the proton rich side of the Segré chart. The numbers listed have been determined using the 2-dimensional gate described before. The final values of the efficiencies have been scaled by the correction factor that has been explained in Sec. 3.2, in such a way that $\varepsilon'_{mn} = \varepsilon_{mn} f^m$, where m is the multiplicity of neutrons and f stands for the correction factor.

Table 3: One-, two- and three-neutron detection efficiencies obtained from simulations of a ^{252}Cf source for the different detector configurations. Errors quoted are statistical.

Geometry	ε'_{1n} [%]	ε'_{2n} [%]	ε'_{3n} [%]
Neutron Wall (NW)	8.81 (6)	0.50 (4)	0.021 (13)
NW + NEDA	13.55 (5)	1.371 (23)	0.125 (12)
NW-ring + NEDA	14.68 (5)	1.743 (21)	0.182 (11)

According to the results of the simulations, this early NEDA - Neutron Wall implementation will provide a substantial improvement in terms of efficiency. The numbers listed in Table 3 show the results of the simulations using a ^{252}Cf source. The fission of ^{252}Cf results in emission of fast neutrons - which are in the same energy range as the neutrons emitted from a fusion-evaporation reaction. The average multiplicity of neutrons from spontaneous fissions of the ^{252}Cf source is

Table 4: One-, two- and three-neutron efficiencies obtained from simulations of a fusion-evaporation reaction ^{58}Ni + ^{56}Fe at 220 MeV for the different detector configurations. Errors quoted are statistical.

Geometry	ε'_{1n} [%]	ε'_{2n} [%]	ε'_{3n} [%]
Neutron Wall (NW)	26.00 (5)	3.93 (10)	0.55 (14)
NW + NEDA	28.70 (5)	6.37 (11)	1.66 (12)
NW-ring + NEDA	31.30 (5)	7.62 (11)	1.89 (11)

3.10(0.18) according to Ref. [25], which makes it interesting for the verification of the neutron multiplicity counting. The results show the advantage of the configurations, in particular, the efficiency increment in the cases where the NEDA detectors are used, especially for two- and three-neutron multiplicities. For an isotropic distribution of neutrons, the increase of efficiency should be proportional to the increase in solid angle coverage, but the configurations involving the NEDA detectors show better performance figures. The results of the fusion-evaporation simulations in Table 4, show that the two-neutron efficiency for the NW + NEDA and NW-ring + NEDA configuration is predicted to be a factor 1.63(5) and 1.95(1), respectively, larger than what is obtained with NW alone. For the three-neutron efficiency the increase is a factor of 3.0(1.7) and 3.4(1.9) for NW + NEDA and NW-ring + NEDA, respectively, compared to NW alone. The NEDA detectors have a larger intrinsic neutron detection efficiency due to their larger depth (20 cm compared to 15 cm for NW). The measured number of photoelectrons per MeV is about 3 times larger for the NEDA detectors compared to the NW detectors [7], which will provide a better neutron-γ discrimination performance. Therefore, in order to benefit from the better performance of the NEDA detectors compared to the NW detectors, the best configuration is the one with the NEDA detectors placed at the forward angles, NW-ring + NEDA shown in Fig. 7-b, where the energy and intensity of the neutrons is largest.

5 Summary

The identification of rare neutron-deficient evaporation residues produced by fusion-evaporation reactions requires a high efficiency for detection of multiple neutrons. This can be achieved by using a detector array with a large solid angle coverage, high granularity and high efficiency. The optimisation of these quantities drove the design of the new NEutron Detector Array, NEDA. The conceptual design of an early implementation of NEDA together with the Neutron Wall, to be coupled to AGATA at GANIL has been described in this work. Two configurations have been discussed: one consists of 50 NEDA detectors and 50 Neutron Wall detectors covering 1.63π sr solid angle and the other consists of 51 NEDA detectors and 45 Neutron Wall detectors covering 1.6π sr solid angle. The performance figures of these two configurations were studied by using a fusion-evaporation event generator that has been discussed an validated in this paper with experimental data. The results of the present work show that the proposed NW-ring + NEDA setup will provide a sizeable improvement compared to the Neutron Wall alone for the detection of multiple neutrons emitted in fusion-evaporation reactions.

6 Acknowledgements

References

[1] B. Cederwall *et al.*, Nature **469** (06 January 2011) 68-71.

[2] Ö. Skeppstedt *et al.*, Nuclear Instruments & Methods In Physics Research Section A **421** (1999) 531-541.

[3] J. Ljungvall *et al.*, Nuclear Instruments & Methods In Physics Research Section A **528** (2004) 741-762.

[4] D. Sarantites *et al.*, Nuclear Instruments & Methods In Physics Research Section A **530** (2004) 473-492.

[5] F.J. Egea Canet *et al.*, IEEE Transactions on Nuclear Science **62** Issue 3 (2015) 1056-1062.

[6] F.J. Egea Canet *et al.*, IEEE Transactions on Nuclear Science **62** Issue 3 (2015) 1063-1069.

[7] V. Modamio *et al.*, Nuclear Instruments & Methods In Physics Research Section A **775** (2015) 71-76.

[8] F. J. Egea *et al.*, IEEE Transactions on Nuclear Science **60** (2013) 3526-3531.

[9] P.-A. Söderström *et al.*, Nuclear Instruments & Methods In Physics Research Section A **594** (1) (2008) 79-89.

[10] X. Luo *et al.*, Nuclear Instruments & Methods In Physics Research Section A **767** (2014) 83-91

[11] G. Jaworski *et al.*, Nuclear Instruments & Methods In Physics Research Section A **673** (2012) 64-72.

[12] S. Akkoyun *et al.*, Nuclear Instruments & Methods In Physics Research Section A **668** (2012) 26-58.

[13] J. Simpson, et al. Acta Physica Hungarica: Heavy Ion Physica **11** (2000) 159-188.

[14] J.J. Valiente-Dobon et al., Annual Report 2014 (2015) 95-96.

[15] S. Agostinelli *et al.*, Nuclear Instruments & Methods In Physics Research Section A **506** (2003) 250-303.

[16] E. Farnea *et al.*, Nuclear Instruments & Methods In Physics Research Section A **621** (2010) 331-343.

[17] P.R.P. Coelho *et al.* Nuclear Instruments & Methods In Physics Research Section A **280** (1989) 270-272.

[18] J. Gomez del Campo and R.G. Stockstad, Oak Ridge National Laboratory Report No. TM7295 (1981), unpublished.

[19] A. Di Nitto *et al.*, Eur. Phys. J. A **47**, (2011) 83-97.

[20] R. Moro *et al.*, Eur. Phys. J. A **48**, (2012), 159-167.

[21] A.J. Koning and J.P. Delaroche, Nucl. Phys. A **713**, (2003), 231-310.

[22] J. Simpson, Z. Phys. A **358** (1997) 139-143.

[23] A. Di Nitto *et al.*, J. Phys. Conf. Ser. **267** (2011) 012053

[24] J. Cederkäll *et al.*, Nuclear Instruments & Methods In Physics Research Section A **385** (1997) 166-170.

[25] W.W.T. Crane, G.H. Higgins and S.G. Thompson, Phys. Rev. **97** (1955) 242.